Near Surface Geophysics, 2005, 93-99

Using trapped waves for mapping shallow fault zones

V. Shtivelman[1], S. Marco[2], M. Reshef[2], A. Agnon[3] and Y.Hamiel[3,4]

1 The Geophysical Institute of Israel, P.O.Box 182, Lod 71100, Israel. E-mail: vladi@gii.co.il
2 Department of Geophysics and Planetary Sciences, Tel Aviv University, Ramat Aviv, Tel Aviv 69978, Israel
3 Institute of Earth Sciences, Hebrew University of Jerusalem, Jerusalem 91904, Israel.
4 Geological Survey of Israel, 30 Malkhei Israel St., Jerusalem 95501, Israel.

Received ?

ABSTRACT

Recent studies have shown that shallow fault zones can be identified by anomalous behaviour of the wavefield recorded by high-resolution seismic surveys. Analysis of seismic records acquired using off-line shooting geometry, where sources and receivers are located along two separate parallel lines crossing a suspected location of a fault zone, reveals prominent anomalies which may be identified with the waves trapped within the zone. On seismic records, trapped waves usually appear as regular low-frequency high-amplitude wavetrains. In order to facilitate the identification of the trapped-wave-related anomalies, we propose two procedures utilizing specific properties of the trapped waves. The first procedure is based on stacking time-scaled seismic traces in the common-shot and common-receiver domains with the subsequent application of eigenimage analysis. In the second procedure, band-limited spectral energy of time-scaled traces is represented as a map in the source–receiver coordinates. By detecting and mapping trapped-wave anomalies in the source and receiver domains, the spatial location of a fault zone can be estimated by linear interpolation between the locations of the corresponding anomalies on the source and receiver lines.

Application of the above procedures is illustrated by a number of synthetic and real data examples.

INTRODUCTION

Detecting and mapping fault zones in the shallow subsurface is an important problem in a variety of applications, such as construction site investigation, seismic risk assessment, environmental studies, archaeology, etc. Among various geophysical methods used for identifying fault zones, seismic methods play a central role. The technique commonly used for this purpose is a high-resolution reflection method. On reflection sections, fault zones usually appear as areas of poor correlation or discontinuity of shallow reflections. However, it is not always possible to obtain shallow reflections of reasonable quality, especially in tectonically disturbed areas. In such cases, alternative techniques can be tried. Since fault zones are usually composed of poorly consolidated material, they can be expected to have low seismic velocities in comparison with their surroundings, and this feature can be used for their identification. If a fault zone is wide enough and has a significant velocity contrast with the surrounding rocks, it can be detected by a seismic refraction method (Palmer 1980, 1981). Analysis of seismic records sometimes reveals anomalous behaviour of the wavefield that can possibly be related to a fault zone. In particular, recent studies have shown that seismic waves, generated by earthquakes and trapped within large fault zones, can be used to identify the zones (Li and Leary 1990; Li et al. 1990, 1994a, b; Leary et al. 1991; Li and Vidale 1996; Ben-Zion 1998; Ben-Zion et al. 2003; Peng et al. 2003). In these studies, fault zones are usually represented as vertical (or nearly vertical) layers with a lower seismic velocity than the surrounding layers. When a source of seismic energy (an earthquake) operates at some depth within the zone, then the constructive interference of the waves totally reflected from the borders of the zone causes a considerable amplification of the wavefield recorded within the zone (Li and Vidale 1996). Thus, a fault zone serves as a waveguide, trapping seismic energy and causing anomalous behaviour of the wavefield on seismic records, on which trapped waves usually appear after the direct body waves as regular high-amplitude low-frequency dispersive wavetrains (Li and Leary 1990; Peng et al. 2003).

Similar considerations can be applied to the study of small shallow fault zones, using standard seismic acquisition techniques, where both the sources and receivers are located at the surface along lines crossing fault zones (Shtivelman and Marco 2003, paper presented at 9th EEGS meeting, Prague, Czech Republic).

We demonstrate here how the trapped waves generated during high-resolution seismic surveys can be used for detecting and mapping small near-surface fault zones. To facilitate the identification of trapped-wave-related anomalies, we propose two procedures utilizing specific properties of the trapped waves. A number of synthetic and real data examples illustrate the application of the above procedures for mapping shallow fault zones.

IDENTIFYING TRAPPED-WAVE ANOMALIES

The analysis of seismic records acquired by high-resolution surveys with off-line shooting, where the source and receiver lines cross a near-surface fault zone, reveals anomalous behaviour of the wavefield that can be related to the fault zone (Shtivelman and Marco 2003, as above). These anomalies are caused by waves trapped within fault zones, and they are represented by regular high-amplitude low-frequency wavetrains appearing as late arrivals. These properties of the trapped waves can be used for their identification.

In order to represent the anomalous effect of the trapped waves in a compact form that facilitates identification of the anomalies and allows them to be traced continuously along seismic lines (rather than examining separate seismograms), we propose the following two procedures:

1 Since trapped waves appear on seismic records as regular coherent events, we apply horizontal stacking (i.e. stacking with zero moveout) to seismic traces in the common-shot and common-receiver domains. Prior to stacking, in order to enhance late arrivals, all traces are scaled (multiplied) by a t^2-function (where t is the time along the trace). After stacking, in order to enhance events with high horizontal coherence further, we apply eigenimage analysis to the stacked sections, keeping only the first eigenimage (Shtivelman 2003).

2 In order to enhance late arrivals, all traces are scaled by a t-function. For each scaled trace, a Fourier transform is performed, and spectral energy of the trace is computed by summing the power spectrum values within a given range of low frequencies. The resulting value, representing band-limited spectral energy for a given source–receiver pair, is placed as a corresponding element in a matrix in which the rows are the source numbers and the columns are the receiver numbers. After completing the above steps for all traces (i.e. for all possible source–receiver pairs), the resulting matrix is displayed as a map of band-limited spectral energy in the source–receiver coordinates. According to the above steps, the low-frequency high-amplitude late arrivals corresponding to trapped waves are expected to be expressed on the map as prominent spatially localized anomalies.

The following synthetic and real data examples illustrate the application of the above procedures.

SYNTHETIC EXAMPLES

We consider three-dimensional models in which a fault zone is represented as a vertical layer with velocity 1000 m/s, located between two layers with velocities 1500 m/s and 2000 m/s (Fig. 1a). The acquisition geometry used for the modelling (Fig. 1b)

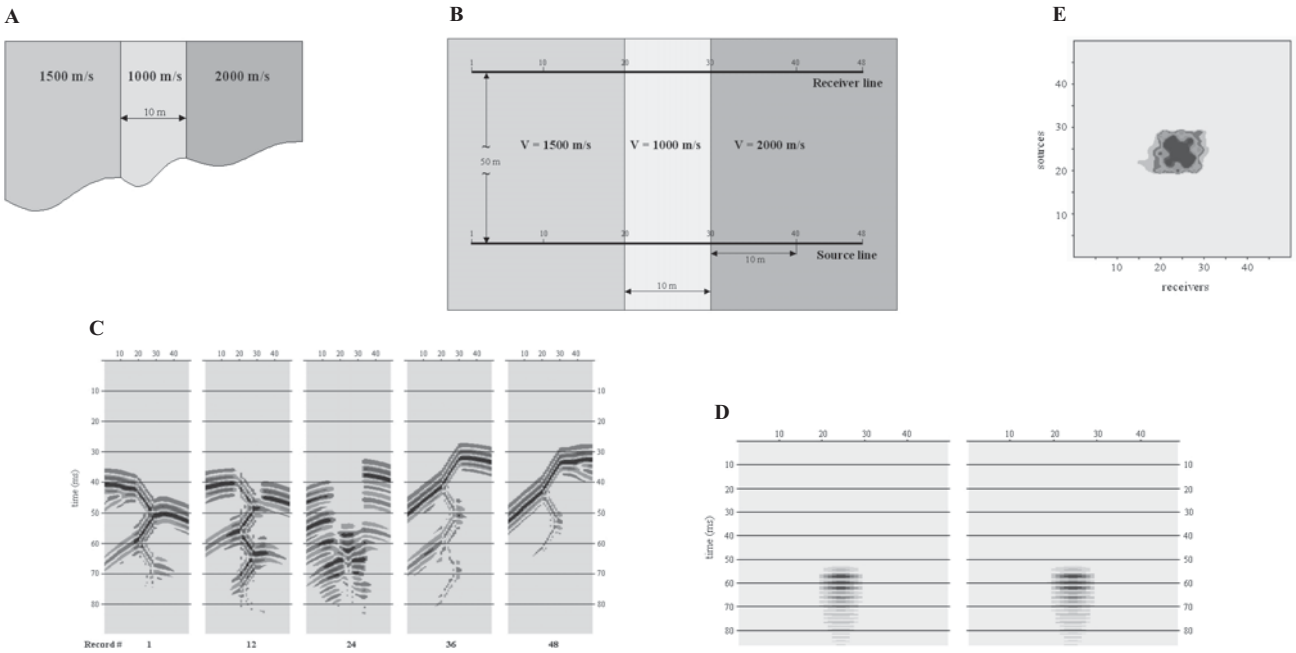

FIGURE 1

Model 1. (a) Vertical section of a three-dimensional model with a fault zone represented as a vertical layer with velocity 1000 m/s. (b) Schematic representation of the acquisition geometry used for the modelling (plan view). (c) Five synthetic seismograms computed for the source locations marked below the records. (d) Common-shot (left) and common-receiver (right) stacked sections. (e) Map of spectral energy in the range 0–70 Hz.

included two parallel lines, located at the surface of the model and crossing the fault zone between stations 20 and 30, as shown in the figure. Along one of the lines (the source line), a source was applied at 48 points, while 48 receivers were located along the second line (the receiver line). The distance between the lines was 50 m; the source and receiver spacing was 1 m. For each model, 48 synthetic seismograms were computed by 3D acoustic modelling using the method of finite differences. The source function was a Ricker wavelet with a dominant frequency of 150 Hz.

Model 1

The model in the first synthetic example includes a 10 m wide fault zone exposed at the surface (Fig. 1a). Figure 1(c) shows five seismograms computed for the source locations marked below the records. We can see that the central seismogram (record #24) displays a wavefield anomaly appearing at times exceeding 50 ms and apparently related to the waves trapped within the zone. Note that the anomaly is localized in the area where both the source and receivers are located within the fault zone.

Figure 1(d) represents common- shot and common-receiver stacked sections obtained for the model of Fig. 1(a) according to the procedure described above. Both sections display well-defined trapped-wave anomalies localized in the areas corresponding to the fault zone location.

Figure 1(e) shows a map of spectral energy obtained for the model of Fig. 1(a) within the frequency range 0–70 Hz. The figure displays a prominent anomaly, localized within the ranges of the sources and receivers, corresponding to the fault zone location.

Model 2

The model in the second synthetic example is similar to the first one but in this case the layer system is overlain by a 5 m thick, horizontal low-velocity layer of velocity 500 m/s (Fig. 2a). The seismograms computed for the model (Fig. 2b) show a dramatic change in data character along the line. In particular, the central seismogram (record #24) displays a long regular high-amplitude wavetrain, appearing at times exceeding 60 ms and related to the waves trapped within the fault zone. The anomalous effect of the trapped waves is also quite prominent on the common-shot and common-receiver stacked sections (Fig. 2c) and on the map of spectral energy (Fig. 2d) where the anomaly is well localized within the area corresponding to the fault zone.

Selection of the proper frequency range for the map of spectral energy can be made on the basis of the frequency content of the trapped waves (as compared to other events) and the character of the anomaly obtained. If the fault zone does not change much between the source and receiver lines, the anomaly can be expected to have a shape close to a square. If the frequency range selected is too narrow or too wide, the shape of the anomaly may be quite different from a square: for example, it may appear as a strip orientated along one of the diagonals of the map. Figure 2(e) represents two examples of the map of spectral energy computed for Model 2: the left one is a narrow-band version (with a

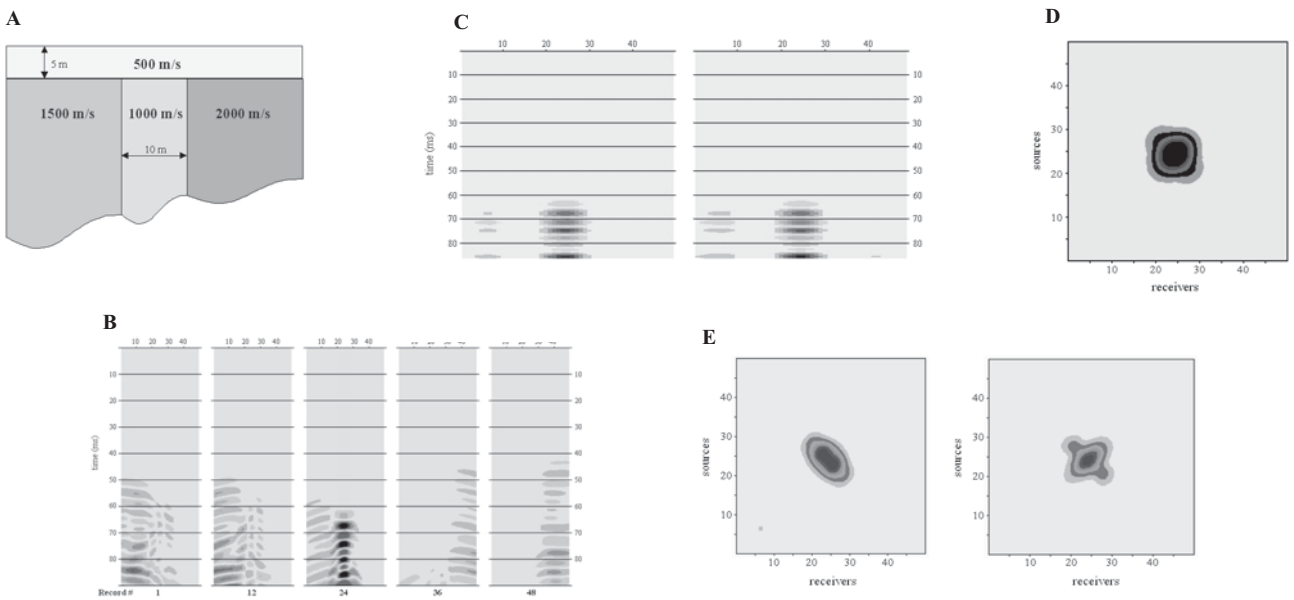

FIGURE 2

Model 2. (a) Vertical section of a three-dimensional model similar to that of Fig. 1(a), but including an overlying low-velocity layer. (b) Five synthetic seismograms computed for the source locations marked below the records. (c) Common-shot (left) and common-receiver (right) stacked sections. (d) Map of spectral energy in the range 0–120 Hz. (e) Two examples of the map of spectral energy obtained in different frequency ranges: left – a narrow-band version (high-cut frequency of 60 Hz), right – a broad-band version (high-cut frequency of 180 Hz). Compare with Fig. 2(d).

high-cut frequency of 60 Hz) and the right one is a broad-band version (with a high-cut frequency of 180 Hz). In the first case, the anomaly appears as a strip stretched along the –45° diagonal, whereas in the second case the anomaly is orientated along the +45° diagonal. Compare these examples with the map shown in Fig. 2(d), which was obtained within the proper frequency range (with a high-cut frequency of 120 Hz), where the anomaly has the shape of a square located within the fault zone boundaries in both the source and receiver domains.

The synthetic examples considered show that the proposed procedures can facilitate the identification of trapped-wave anomalies related to shallow fault zones. In those cases when the anomalies can be reliably identified in both the source and receiver domains, a spatial position of the fault zone can be estimated by locating the corresponding ranges of the anomalies on the source and receiver lines and using linear interpolation between the locations.

REAL DATA EXAMPLES

The data for the following examples were acquired at three sites located in different areas of Israel (Fig. 3). The seismic survey carried out at each site included two parallel lines designed to cross the presumed location of a fault zone. Each line was 47 m long and the distance between the lines was about 50 m. 48 receivers at 1 m spacing were located along one of the lines (the receiver line) and a source of seismic energy was applied every 1 m along the second line (the source line). As a result, the seismic data acquired at each site consisted of 48 records with 48 traces per record. At sites 1 and 2, the Digipulse (a truck-mounted accelerated weight drop) was used as the source, whereas at site 3, the source was a sledgehammer striking an aluminium plate. In addition, a refraction survey was carried out along the receiver line at site 3. The refraction data were processed and interpreted using the generalized reciprocal method (Palmer 1980, 1981).

Site 1

FIGURE 3
Schematic location of seismic surveys at three sites.

The first example is from the Ateret site located in the Jordan valley in northern Israel (Fig. 3). The site is an archaeological mound situated on a Pleistocene basalt flow covering a Plio-Pleistocene lacustrine chalky limestone sequence. Several echelon fault strands rupture a synclinal structure developed in the young sediments. The mound contains structures and artefacts from various historical periods. Offsets observed on walls of the Crusader and Ottoman structures are related to surface ruptures caused by the 1202 and 1759 earthquakes and indicate the existence of a near-surface fault zone.

Figure 4(a) shows six records from the survey carried out at the site. Record 20 (corresponding to shot station 20 on the source line) displays a low-frequency high-amplitude wavetrain, apparently related to trapped waves, appearing within the receiver range 27–37 and at times exceeding 300 ms. The common-

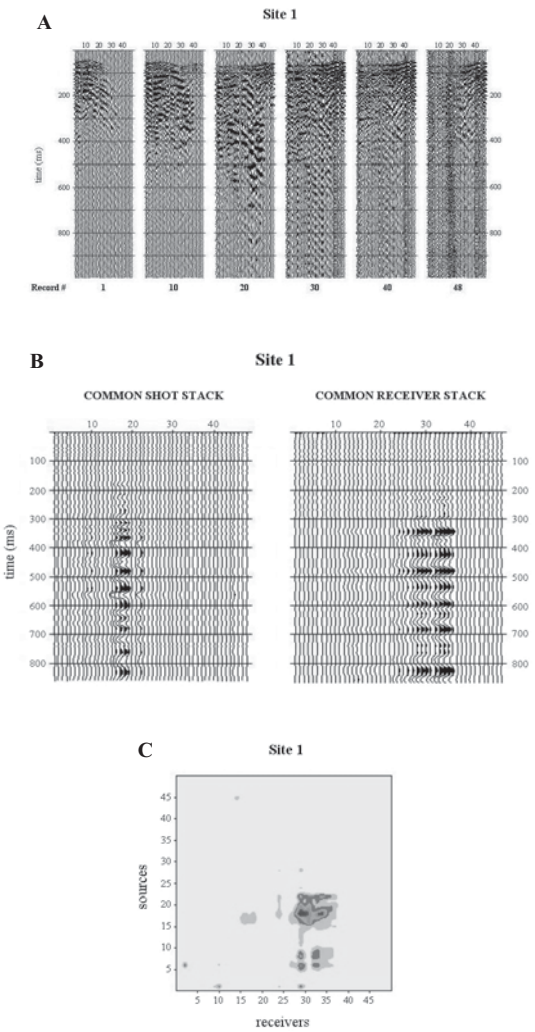

FIGURE 4
Site 1. (a) Six records shown with true relative amplitudes. The record numbers shown below correspond to the shot position along the source line. (b) Common-shot (left) and common-receiver (right) stacked sections. (c) Map of spectral energy in the range 0–30 Hz.

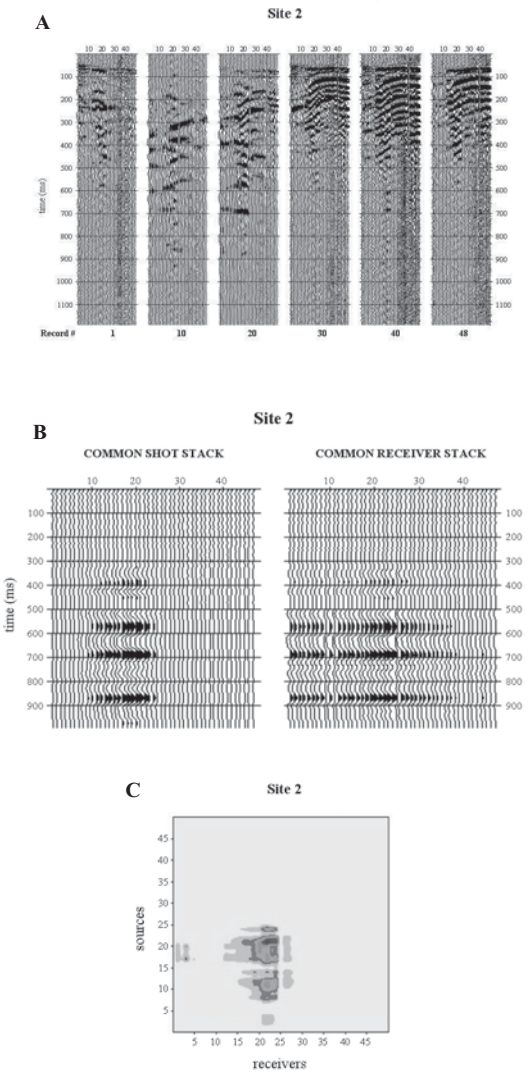

FIGURE. 5
Site 2. (a) Six records shown with true relative amplitudes. The record numbers shown below correspond to the shot position along the source line. (b) Common-shot (left) and common-receiver (right) stacked sections. (c) Map of spectral energy in the range 0–30 Hz.

shot and common-receiver stacked sections (Fig. 4b) display trapped-wave-related anomalies in the ranges 16–22 and 24–36, respectively. On the spectral energy map obtained within the frequency range 0–30 Hz (Fig. 4c), an anomaly appears within the same range of sources (16–22) but within a slightly different range of receivers (27–37). Based on these results, we can estimate the spatial location of the fault zone at the site as being bordered by two lines: the left line passes through station 16 on the source line and somewhere between stations 24 and 27 on the receiver line, and the right line passes through station 22 on the source line and stations 36 and 37 on the receiver line.

Site 2

This example is from a site situated in Upper Galilee, to the north of the town of Kiriat Shemona (Fig. 3). The site is located in the area of a contact between two geological units, Palaeocene-Early Eocene marls to the west and Pleistocene basalt to the east. Recent studies have identified the contact as a fault. Certain indications of several small near-surface fault zones can be found at the site. In particular, about 20 m to the east of the contact, a 1.5 m wide fault zone is exposed within the basalt.

Figure 5(a) shows six records from the survey carried out at the site. On records 10 and 20, at times exceeding 290 ms, we can see high-amplitude low-frequency events that may be identified as trapped waves. The common-shot stacked section (Fig. 5b, left) displays a distinctive anomaly in the range of approximately 9–22; no definite trapped-wave-related anomaly could be detected on the common-receiver stack (Fig. 5b, right). The map of spectral energy (Fig. 5c) displays two anomalies located approximately within the same range of receivers (18–25) and in the source ranges 8–12 and 16–22. The existence of two anomalies in the source domain may indicate one of two possibilities: either they are actually one anomaly corresponding to the anomaly identified on the common-shot stack (stations 9–22), or the fault zone identified on the receiver line splits into two separate zones crossed by the source line. In any case, the left border of the fault zone area can be defined by a line passing between source stations 8 and 9 and through receiver station 18, whereas the right bordering line passes through source station 22 and receiver station 25.

Site 3

This site is located in the Eilat mountains, a desert area of southern Israel, where several fault zones are exposed at the surface (Fig. 3). The survey was conducted within a dry stream bed at Nahal Shlomo. At the site, a north-striking normal fault separates Late Cretaceous marine sediments (limestone) to the west from Precambrian basement rocks (granite) to the east. At several locations along the fault, a 5–8 m wide fault zone is exposed. The zone is composed of angular breccia, containing unsorted, poorly consolidated fine-to-boulder-sized rock fragments, and bordered by seemingly undisturbed country rocks. In a part of the study area, the fault is covered by alluvial deposits with a thickness of up to 10 m.

Figure 6(a) shows six records from the survey carried out at the site. We can see a dramatic change in the data character along the line. In particular, the central part of record #30, approximately between stations 16 and 30 and at times exceeding 280 ms, displays a long regular low-frequency high-amplitude wavetrain that can apparently be identified with the waves trapped within the fault zone. The common-shot stack (Fig. 6b) shows an anomaly located between shot stations 22 and 32. Unfortunately, both the common-receiver stack and the spectral-energy map failed to produce any definite anomaly that could be related to trapped waves. On the other hand, the refraction section obtained

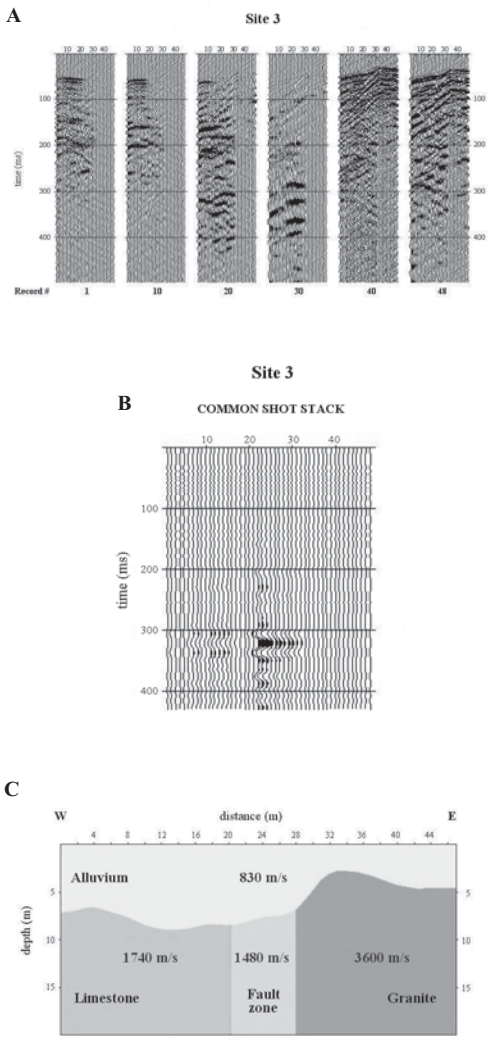

FIGURE 6
Site 3. (a) Six records shown with true relative amplitudes. The record numbers shown below correspond to the shot position along the source line. (b) Common-shot stacked section. (c) Refraction depth section along the receiver line.

along the receiver line (Fig. 6c) reveals a distinctive low-velocity zone between receiver stations 20 and 28. The zone is bordered by weathered limestone to the left and granite to the right. Since it is difficult to identify clearly the left border of the trapped wave anomaly appearing on the seismograms (Fig. 6a) and since the presence of a 7–8 m thick, low-velocity layer above the fault zone (Fig. 6c) apparently tends to extend the anomaly beyond the borders of the zone, we assume that in this case it is more reliable to define the fault zone location on the receiver line according to the refraction section, i.e. between receiver stations 20 and 28. Thus, the spatial position of the fault zone can be estimated as being limited to the left by station 22 on both the source and receiver lines, and to the right by a line passing through receiver station 28 and source station 32.

The above examples show that in some cases, when a common-shot stack displays a well-defined trapped-wave-related anomaly, the common-receiver stack may fail to produce any indication of the anomaly. This difference between the source and receiver domains may be related to the differences in the wavefield character represented by the corresponding stacked sections. Under certain conditions, a common-shot stack can be regarded as representing a zero-offset section (see, for example, Loewenthal *et al*. 1999), whereas a common-receiver stack can be considered as a kind of a plane-wave approximation. This leads to the differences in the specific features (in our case, trapped-wave anomalies) appearing on the sections.

SUMMARY

Shallow fault zones can be identified by trapped-wave anomalies appearing on the data of high-resolution seismic surveys using off-line shooting. The anomalies correspond to the areas where both the sources and receivers are located within the fault zone.

The identification of the trapped-wave anomalies can be facilitated by applying the procedures described above, as illustrated by synthetic and real data examples.

The spatial location of fault zones can be estimated using linear interpolation between the locations of the trapped-wave anomalies detected on the source and receiver lines.

ACKNOWLEDGEMENTS

The authors are grateful to the Ministry of National Infrastructures for financial support and to the Geophysical Institute of Israel for permission to publish this paper.

REFERENCES

Ben-Zion Y. 1998. Properties of seismic fault zone waves and their utility for imaging low-velocity structures. *Journal of Geophysical Research* **103**, 12567–12585.

Ben-Zion Y., Peng Z., Okaya D., Seebar L., Armbruster J.G., Ozer N., Michael A.J., Baris S. and Aktar M. 2003. A shallow fault-zone structure illuminated by trapped waves in the Karadere-Duzce branch of the North Anatolian Fault, western Turkey. *Geophysical Journal International* **152**, 699–717.

Leary P.C., Igel H. and Ben-Zion Y. 1991. Observation and modeling of fault zone seismic trapped waves in aid of precise precursory microearthquake location and evaluation. *Proceedings of Conference on Earthquake Prediction: State-of the Art,* Strasbourg, France, pp.

Li Y.-G., Aki K., Adams D., Hasemi A. and Lee W.H.K. 1994a. Seismic guided waves trapped in the fault zone of the Landers, California, earthquake of 1992. *Journal of Geophysical Research* **99**, 11705–11725.

Li Y.-G. and Leary P.C. 1990. Fault zone trapped seismic waves. *Bulletin of the Seismological Society of America* **80**, 1245–1271.

Li Y.-G., Leary P.C., Aki K. and Malin P. 1990. Seismic trapped modes in the Oroville and San Andreas fault zones. *Science* **249**, 763–766.

Li Y.-G. and Vidale J.E. 1996. Low-velocity fault –zone guided waves: numerical investigations of trapping efficiency. *Bulletin of the Seismological Society of America* **86**, 371–378.

Li Y.-G., Vidale J.E., Aki K., Marone C. and Lee W.H.K. 1994b. Fine structure of the Landers fault zone; segmentation and the rupture process. *Science* **256**, 367–370.

Loewenthal D., Buchen P., Kagansky A. and Koren I. 1999. Zero moveout (ZMO) stacking. *Geophysics* **64**, 567–571.

Palmer D. 1980. *The Generalized Reciprocal Method of Seismic Refraction Interpretation*. Society of Exploration Geophysicists, Tulsa, OK.

Palmer D. 1981. An introduction to generalized reciprocal method of seismic refraction interpretation. *Geophysics* **46**, 1508–1518.

Peng Z., Ben-Zion Y., Michael A.J. and Zhu L. 2003. Quantitative analysis of seismic fault zone waves in the rupture zone on the 1992 Landers, California, earthquake: evidence for a shallow trapping structure. *Geophysical Journal International* **155**, 1–21.

Shtivelman V. 2003. Improving the resolution of shallow seismic sections using eigenimage analysis. *Near Surface Geophysics* **1**, 149–154.